Journal of Coastal Research	33	2	243–253	Coconut Creek, Florida	March 2017

Determining Dredge-Induced Turbidity and Sediment Plume Settling within an Intracoastal Waterway System

Ping Wang[†]* **and Tanya M. Beck**[‡]

[†]Coastal Research Laboratory
School of Geosciences
University of South Florida
Tampa, FL 33620, U.S.A.

[‡]Coastal and Hydraulics Laboratory
U.S. Army Engineer Research and Development Center
Vicksburg, MS 39180, U.S.A.

www.cerf-jcr.org

www.JCRonline.org

ABSTRACT

Wang, P. and Beck, T.M., 2017. Determining dredge-induced turbidity and sediment plume settling within an intracoastal waterway system. *Journal of Coastal Research,* 33(2), 243–253. Coconut Creek (Florida), ISSN 0749-0208.

The intracoastal waterway (IWW) is a continuous navigation channel that often extends across seagrass beds and other sensitive habitats throughout the Gulf and Atlantic Coast estuaries of the United States. Turbidity increase associated with an IWW dredging operation in west-central Florida and subsequent dredge plume subsidence were measured with optical backscatter sensors and acoustic Doppler velocimeters, which also measured *in situ* wave and current conditions. The field experiments were conducted over a dense seagrass bed. Sediment in the study area is dominantly composed of fine, well-sorted quartz sand, typical of Florida estuaries. The dredge plume temporally increased the turbidity to more than 400 mg/L around a midwater depth. The settling of the dredge plume and sediment resuspension were calculated with commonly used empirical formulas for noncohesive sediments and compared with field observations. The relatively energetic conditions generated by frequent boat wake did not result in significant resuspension and remixing of the suspended sediments and had minor influence on the settling time of the dredge plume. Findings from this study may provide information on understanding potential impacts of dredging on seagrass beds.

ADDITIONAL INDEX WORDS: *Channel dredging, estuaries, dredge plume, settling velocity, boat wake, sediment transport, seagrasses, submerged aquatic vegetation (SAV), Florida.*

INTRODUCTION

Dredging and placement of dredged material are often necessary to maintain and improve waterways for safe navigation. Dredging operations may result in a temporary increase in concentration of sediments within the water column (Schoellhamer, 1996, 2002a,b), which may have various impacts on the marine environments. The seagrass bed, a type of submerged aquatic vegetation (SAV), is one of the important marine habitats sensitive to sediment concentration variations (Moore, Wetzel, and Orth, 1997; Onuf, 1994; Ralph *et al.*, 2006). Major potential impacts on seagrass beds from dredging include physical removal or burial of seagrasses and temporary increases in suspended-sediment concentration (Erftemeijer and Lewis, 2006). The latter may result in increased light attenuation, which can negatively affect seagrasses' health (Koch, 2001; Robert, Matthew, and Graeme, 2006).

An increased suspended-sediment concentration associated with dredging, or dredge plumes, can be generated by two aspects of the operation: (1) extraction and agitation of sediment at the bottom substrate and (2) overflow from the dredge hopper bin or containment vessel (Pennekamp *et al.*, 1996; USACE Staff, 2015). In other words, an elevated sediment concentration in the water column can be introduced from both the bed and the water surface.

DOI: 10.2112/JCOASTRES-D-16-00083.1 received 9 May 2016; accepted in revision 8 July 2016; corrected proofs received 28 August 2016; published pre-print online 21 October 2016.
*Corresponding author: pwang@usf.edu

For cutterhead-suction hopper dredges, overflow from the hopper bin can be the dominant contributor to a dredge plume for mostly fine, sand-size sediment (USACE Staff, 2015). This type of suspended-sediment input is introduced by overflow at the water surface and is subsequently mixed into the water column. Three primary factors act upon the sediment mixing: advection–diffusion in the ambient environment, vessel-induced currents, and settling of the sediments. The suspended-sediment input from the extraction process is initiated at the bottom and is mixed upward through the water column by the turbulence associated with the dredge operation, in addition to the ambient currents and particle advection and diffusion (USACE Staff, 2015). Understanding of the mechanisms of transport and deposition of a dredge plume over SAV and their subsequent temporal impact is quite limited.

Seagrasses distribute broadly in the back-barrier estuaries along coastal Florida, United States. The intracoastal waterways (IWWs), extending hundreds of kilometers through the back-barrier bays of the Gulf and Atlantic Coasts of the United States, often cut through seagrass beds. Maintenance dredging of the IWW and associated dredge-induced sediment plumes may have significant influence on these submerged aquatic habitats. In this study, various field measurements were conducted during an IWW maintenance dredging project by the U.S. Army Corps of Engineers (USACE) to quantify sediment suspension and subsequent settling in the vicinity of the extraction location. Based on these field measurements, a dredge plume that settled over adjacent seagrass beds and the associated controlling factors on sediment settling and resuspension are examined. Time series of sediment concentrations were measured using three turbidity sensors. Hydrodynamic

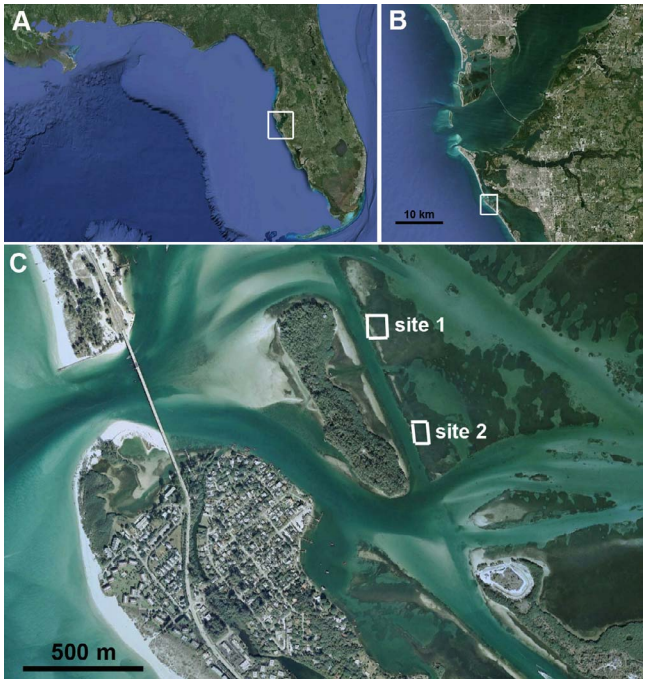

Figure 1. Study area map. (A) The NE Gulf of Mexico, (B) the mouth of Tampa Bay, and (C) a close-up of the study area, illustrating a stretch of the IWW extending (or previously dredged) through a seagrass bed. The measurement sites were located along the navigation channel over the seagrass bed. (Color for this figure is available in the online version of this paper.)

conditions were measured using an acoustic Doppler velocimeter (ADV). Underwater photos were taken every 10 seconds, in addition to videos, to visualize the sediment plume evolution.

The main goals of this study are to quantify the following: (1) increased sediment concentration over a seagrass bed associated with a nearby (within 100 m) hopper-dredging operation, (2) potential sediment concentration fluctuations associated with boat wakes, and (3) settling of the dredging plume. Spatial patterns of advection and diffusion of the plume are beyond the scope of this study. Observation, collection, and testing of seagrass species in the study area were also outside the scope of this research. Erftemeijer and Lewis (2006) summarized numerous potential environmental impacts of dredging on seagrasses. This study focuses on one of the factors, *i.e.* settling of dredging-induced turbidity plumes.

Study Area

The study area is located in west-central Florida, just south of the mouth of Tampa Bay, where the IWW extends along the back-barrier bay (Figure 1). The studied section of the IWW cuts across the flood tidal delta of Longboat Pass, a small mixed-energy tidal inlet just south of the mouth of Tampa Bay. This portion of the flood tidal delta consists of an emergent mangrove island surrounded by dense seagrass beds (Figure 1C) composed of predominantly manatee grass *(Syringodium filiforme)* with a mix of turtle grass *(Thalassia testudinum)*. The dense seagrass canopy extends roughly 20 cm above the

Figure 2. The USACE special operations hopper dredge, Murden, passing in front of the measurement site (metal pole at the bottom of the picture). The slurry was pumped into the container of the dredge. The overflow is visible along the side of the vessel. (Color for this figure is available in the online version of this paper.)

bottom. Overall, the study area is well sheltered with low wave energy. The greater study area is characteristic of a mixed tidal regime (Wang and Beck, 2012). The spring tide is typically diurnal with a range of roughly 0.8 to 1.2 m, while the neap tide is semidiurnal with a range of 0.4 to 0.5 m. Tidal currents at the study site are generally less than 0.2 m/s and typically 0.05 to 0.15 m/s based on the measurements by this study.

Two sets of field measurements were conducted. The first set, at Site 1 in Figure 1C, was conducted on March 15, 2013. No dredging activities occurred during that day. These data provide background information about ambient currents and turbidity during a day with low wind energy ($<$5 m/s based on a nearby National Oceanic and Atmospheric Administration measurement station) similar to the date with measurements of dredge-induced turbidity plumes. The second set of field measurements, at Site 2 in Figure 1C, was conducted on March 17, 2013, during and adjacent to the dredging operation (Figure 2). The USACE special operations vessel, the Murden, extracts bottom sediment through suction and pumps the slurry into the hopper container within the vessel. The overflow is discharged from the sides of the vessel during operation until the bin is filled with settled sediment. The water depth at the experiment site ranged from 0.5 to 1.5 m, because it is located on a shallow, flat bay area adjacent to the roughly 3-m-deep, artificial IWW channel.

The weather conditions during both the March 15 and the March 17, 2013, experiments were largely calm, with small wind-generated, choppy waves generally less than 0.1 m in height. The following discussions focus on the March 17 measurement, when dredging occurred. The experiment was conducted during a rising tide. The tidal-driven flow measured by the current meters used in this study was mostly less than 0.1 m/s. The only relatively energetic conditions experienced during the study were boat wakes generated by frequent passages of recreational vessels on a Sunday afternoon. The study area is not located within a no-wake zone of the IWW. The recreational vessels moving at normal operation speed generated boat-induced waves often exceeding 0.2 m in height.

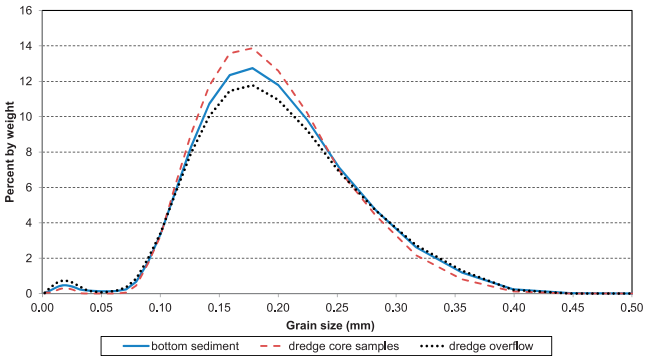

Figure 3. Averaged sediment grain-size distributions, comparing samples from the seabed, within the dredge container, and from the dredge overflow. (Color for this figure is available in the online version of this paper.)

METHODS

The study site was chosen according to the proximity to the dredging activity, the probability of encountering a dredge-induced plume based on daily observations of the dredge Murden's sediment plumes, locations within SAV habitat, and water-depth requirements of the instrumentation. Measurements were conducted at three proximal locations roughly perpendicular to the navigation channel (Figure 1C). Location 1 was directly adjacent to the channel, with a water depth of roughly 1.2 m, and west of the closest dredge position in the channel by 12 m. Location 2 was about 15 m west of the edge of the channel (and Location 1) and at a water depth of about 0.9 m. Location 3 was approximately 5 m west of Location 2 and at a similar water depth but with less seagrass coverage, *i.e.* over a relatively unvegetated substrate. Location 1 was the closest to the dredging operation and is the focus of the following analyses.

At each measurement location, an instrument tripod mounted with a GoPro underwater camera, a scaled rod, and an YSI OMS 600 (optical monitoring system) turbidity sensor measuring suspended-sediment concentration was deployed. In addition, a Nortek Vector ADV, an underwater video camera (GoPro), and an underwater light meter were deployed at Location 1. The results from the light meter measurements are beyond the scope of this paper. An underwater photo was taken every 10 seconds using the scaled rod, located about 50 cm from the camera, as a reference. The ADV sensor measuring three-dimensional current and water depth was sampling continuously at 8 Hz at 50 cm above the bed (or roughly 30 cm above the seagrasses). Tidal currents and wave motions associated with boat wakes were measured by the ADV. Furthermore, the acoustic signal strength, which is proportional to sediment concentration, provided a qualitative measurement of temporal variation of turbidity. Each OMS turbidity sensor was installed 56 cm above the bed (or roughly 40 cm above the seagrasses), sampling continuously at 0.5 Hz. The relatively low sampling rate was not adequate to resolve the sediment-concentration fluctuations associated with boat wakes or wind waves. However, the signal strength from the ADV, sampling continuously at 8 Hz, provided some qualitative information for examining sediment-concentration fluctuations related to boat wakes. The high-frequency wind waves were very small and largely not detectable by the sensor located approximately 60 cm below the water surface.

Sediment samples from the IWW channel substrate, within the dredge container, and from the dredge overflow were collected. Bottom sediment samples were collected using a Petite Ponar grab sampler at locations within the dredge area. The sediment in the overflow was sampled using an extension-arm bottle sampler at the overflow weir. Sediments in the hopper basin were collected using a push core. Typically, a roughly 50-cm core sample was collected. Sediment grain size was analyzed using a Malvern laser sediment profiler. Statistical grain-size parameters were calculated using the moment method. Sediment characteristics at the channel bottom, within the dredge container, and in the overflow are compared.

RESULTS

Because the focus of this paper is to investigate and quantify elevated suspended-sediment concentration within the water column as it relates to the process of dredging, the results here focus primarily on the YSI OMS 600 and the Nortek Vector ADV data and their temporal variations.

Sediment Characteristics

A total of 14 sediment samples were collected during the field measurements on March 17, 2013, to compare sediment properties among sediments on the substrate, in the dredge container, and within the overflow. Ten bottom sediment samples were collected from the dredge area. Sediments in the dredge container are represented by two 50-cm-long sediment core samples. Because overflow from the dredge was expected to be the primary contribution to the plume, two overflow water and sediment samples were collected. Each sample was analyzed for grain-size distribution separately. The average grain-size distribution for the three types of sediment samples, *i.e.* bottom sediment, dredged material in the hopper bin, and overflow slurry, are illustrated in Figure 3.

Sediment in the study area is composed of well-sorted fine sand, typical of the west-central Florida coast. The mean grain size of the sediment from the dredge hopper bin is the coarsest, at 0.175 mm. The average mean sediment grain size at the seabed is slightly (2%) finer at 0.172 mm. The mean grain size of the overflow is the finest at 0.165 mm, or about 6% finer than the sediment in the container, with a slightly higher percentage of silt- and clay-size fractions. The grain-size distribution approximates a normal distribution curve, with a slight coarse tail. Overall, the sediments on the seabed, in the dredge container, and within the dredge overflow are quite similar. This is controlled by the well-sorted fine sand in the greater study area (Wang and Beck, 2012).

Dredging-Induced Suspended-Sediment Concentrations

As the container of the hopper dredge became full, typically within 5 minutes of the start of dredging, the overflow slurry resulted in an increased concentration of suspended sediment in the water column. A direct consequence of the increased suspended particles was substantially reduced visibility (Fig-

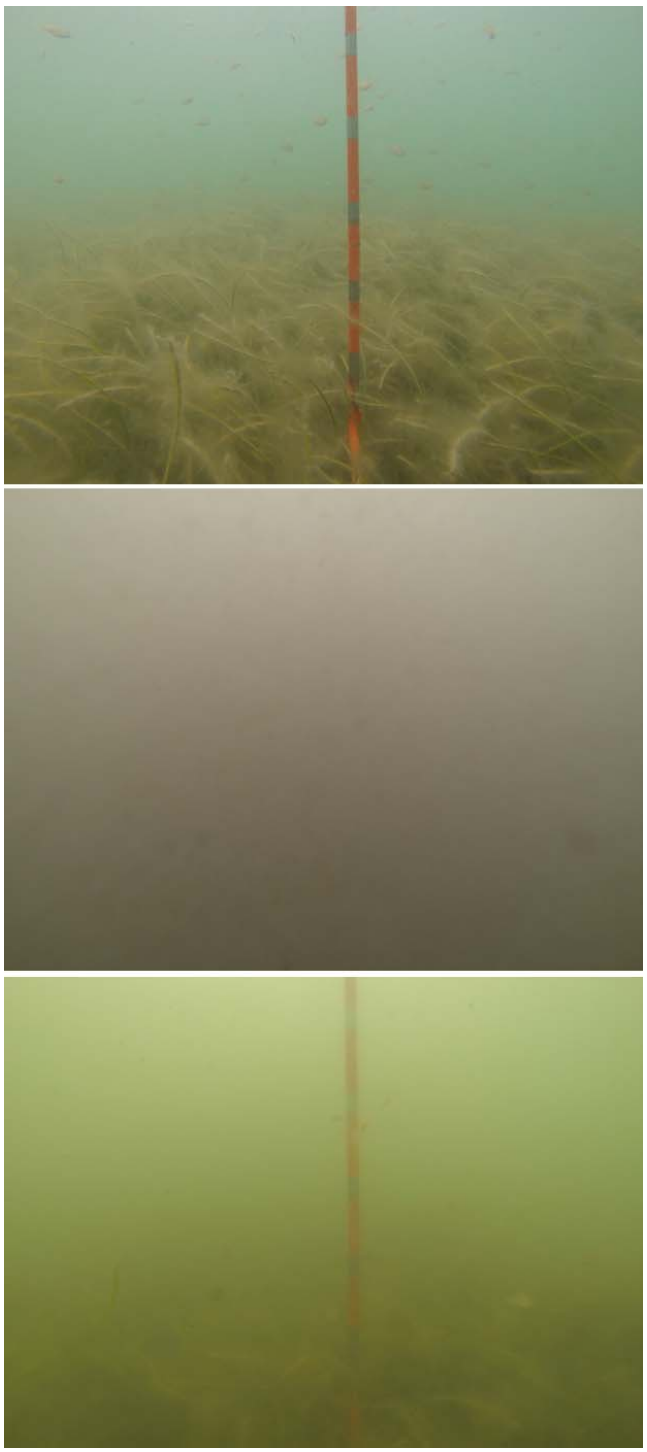

Figure 4. Underwater photos of turbidity increase and decrease during the dredging operation. Upper: Condition before the dredging operation; the dense seagrass extends about 20 cm from the seabed. Middle: Condition at the peak of the dredge turbidity plume; the reference rod about 0.5 m in front of the camera has become invisible. Lower: Condition 50 minutes after the turbidity peak; the visibility has recovered considerably. (Color for this figure is available in the online version of this paper.)

ure 4). At the peak of the plume, the visibility was less than 0.5 m as the scaled rod became invisible (Figure 4, middle panel). Reduced sunlight penetration is one of the main issues concerning the impact of dredging on seagrass beds (Onuf, 1994; Shafer, 1999). As shown in the bottom panel of Figure 4, the visibility improved considerably 50 minutes after the peak of the plume, although it was still less than that at the beginning.

Suspended-sediment concentration was measured using three YSI OMS 600 turbidity sensors sampling continuously at 0.5 Hz during the entire experiment. The three sensors were deployed within 20 m of one another at different water depths, as described earlier. Sensor 1 (at Location 1) was located in the deepest water of approximately 1.2 m on the slope of the navigation channel, around 64 cm below mean water level, and was positioned nearest to the dredging operation (Figure 2). Sensor 1 was also colocated with the Nortek ADV that measured current and wave conditions, particularly those related with boat wakes. Sensor 2 was located on the seagrass bank in water shallower than that of Sensor 1, at a water depth of 0.9 m (approximately 34 cm below mean water level). Sensor 3 was also located on the bank but in a site that had less dense seagrass coverage at a water depth of 0.9 m (approximately 34 cm below mean water level).

Overall, the three turbidity sensors measured a similar temporal pattern of suspended-sediment concentration variations (Figure 5), likely controlled by their proximity. Based on visual observations during the field measurements, the dredge-induced sediment plume arrived at the sensor approximately 15 minutes after the first pass of the vessel in front of the measurement site and peaked around 13:40 local time, or roughly 50 minutes after the dredge's first arrival. The dredging activity occurred along an approximately 150-m stretch of channel directly in front of the sensors. The dredge passed back and forth in front of the sensors six times. The dredging operation lasted approximately 1.5 hours before the dredge discontinued the extraction process and headed to the disposal site.

The turbidity sensors were first tested in the laboratory against distilled water (nephelometric turbidity units, or NTUs, or 0), and against a known standard value of 126 NTU before field deployment. During the field measurements, the sensor readings were compared with direct measurements by pump sampling. Figure 6 plots and provides a linear and third-order polynomial curve fit of the OMS and pump samples data. The third-order polynomial curve fits the measured data considerably better than a linear curve. Perkey, Pratt, and Ganesh (2010) discussed similar regression analyses on pump samples and turbidity and determined that a polynomial fit best represented the trend in turbidity variations.

The third-order polynomial equation, as shown in Figure 6, was used to convert the turbidity sensor data (in nephelometric turbidity units) to sediment concentration in milligrams per liter. Figure 7 illustrates the sediment concentration in milligrams per liter using the third-order polynomial calibration curve for all three YSI OMS 600 sensors. The negative nephelometric turbidity unit readings (Figure 5) indicate that the sediment concentration values fell below the range of

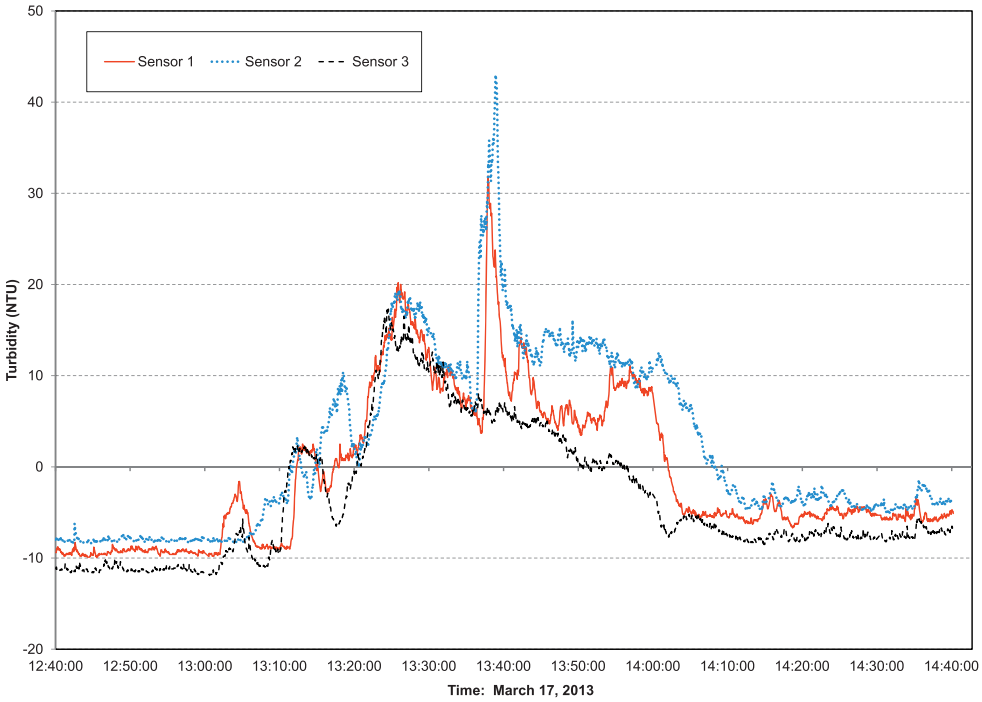

Figure 5. Temporal variations of turbidity (in nephelometric turbidity units) at the three measurement sites. (Color for this figure is available in the online version of this paper.)

operation for the YSI OMS 600 turbidity sensors and therefore were replaced with a concentration of zero in Figure 7.

The peak suspended-sediment concentration induced by the dredging operation reached nearly 450 mg/L briefly, measured by Sensor 2 over a shallow (~0.9 m) seagrass bed (Figure 7). Sensor 1, deployed along the slope of the channel, measured magnitudes and temporal patterns of suspended-sediment concentration similar to those of Sensor 2. Two apparent peaks of elevated suspended-sediment concentrations, around 130 and 280 mg/L, were captured. The two peaks were not directly related to specific passages of the Murden. The vessel passed in front of the sensors six times. The sensors did not capture six separate peaks in suspended concentrations. The nearby Sensor 3 did not capture the second high peak, suggesting substantial spatial variations in the sediment plume, as observed in the field. The slightly longer distance of Sensor 3 to the dredging operation and the temporal characteristics of the settling of the plume, as discussed in the following, are likely attributable to the absence of the second concentration peak (Figure 7).

Water level and current velocity measurements were conducted continuously using the Nortek ADV during the entire deployment period of 3 hours during a rising tide. The time-averaged velocity measured by the ADV was largely less than 0.1 m/s. The acoustic signal strength recorded by the Nortek ADV provided a qualitative measure of sediment concentration, which provided additional concentration data with high temporal resolution, as well as currents and wave data. The ADV is colocated with Sensor 1 along the slope of the channel. Figure 8 compares the average acoustic signal strength from the three receivers (for the three velocity components) with the low-frequency measurements from the Location 1 OMS sensor. Overall, the temporal trends of the two sensors are quite similar, suggesting that the ADV data can be used to qualitatively evaluate the sediment concentration evolution. The ADV sampled at a higher frequency of 8 Hz, as opposed to the 0.5-Hz sampling rate of the OMS sensors. The ADV data are examined here to quantify the potential sediment-concentration fluctuations associated with local

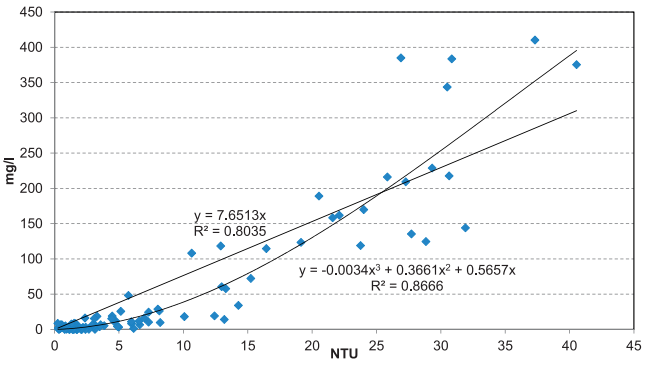

Figure 6. Calibration curves of the OMS turbidity sensors based on pump–suction measurements in the field. A third-order polynomial curve fits the measured data, with an R-squared value of 0.87. (Color for this figure is available in the online version of this paper.)

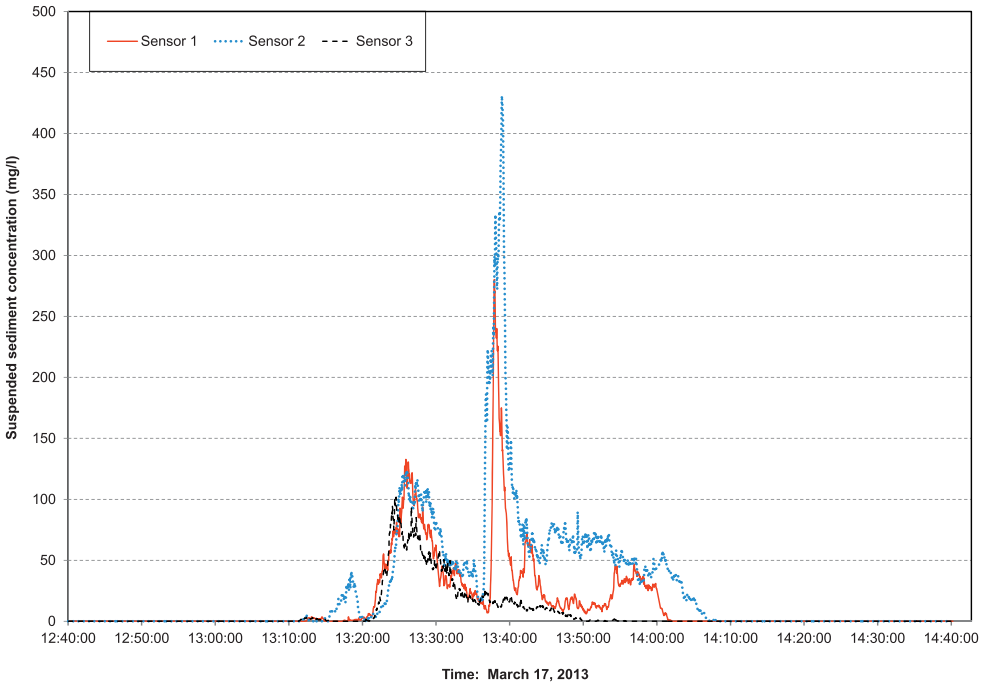

Figure 7. Temporal variations of turbidity in units of milligrams per liter at the three measurement sites. (Color for this figure is available in the online version of this paper.)

hydrodynamic conditions such as wind waves and boat wakes, as discussed in the following.

DISCUSSION

The dredging site is located in an area with weak tidal-driven flow despite its proximity to a tidal inlet. In general, seagrass beds tend to distribute in areas with relatively low wave and tidal energy for seeding (Robert, Matthew, and Graeme, 2006). With measured currents not exceeding 0.1 m/s, advection of the turbidity plume by tidal, wind, or vessel-driven currents was not significant for this case. However, the measurements were conducted on a Sunday afternoon with significant recreational vessel traffic adjacent to the study site. The influence of vessel-induced boat wake on the turbidity fluctuation and plume settling is examined in the following.

Influence of Hydrodynamics on Turbidity Fluctuation

Because of the limited fetch and extensive shallow water covered by seagrass beds (Figure 1), wind-generated waves were small and significantly dissipated in the study area. However, because of the proximity to the IWW and a tidal inlet, the study site is subject to a significant amount of recreational vessel traffic, generating relatively energetic wave conditions. Figure 9 illustrates two examples of boat wakes that had occurred immediately after the two sediment-concentration peaks. The velocity measurements were conducted around 0.6 m below the water surface, and considerable depth attenuation occurred for the high-frequency boat wake. Based on linear wave theory, the frequency-dependent depth attenuation factor $K(f)$ can be calculated as (Wang and Stone, 2004)

$$K(f) = \frac{\cosh[k(z_s + h)]}{\cosh(kh)} \quad (1)$$

where wave number $k = 2\pi/L$ (in reciprocal meters); L is the wave length (in meters); z_s is depth (in meters) of the sensor below the water surface (negative downward), –0.6 m in this case; and, h is the water depth at the measurement site, 1.2 m in this case. The wave length L in shallow water can be calculated based on the dispersion equation as

$$L = \frac{g}{2\pi} T^2 \tanh \frac{2\pi h}{L} \quad (2)$$

where T is the wave period (in seconds) and g is the gravitational acceleration (in meters per square second). Based on Equations (1) and (2), the wave orbital velocity at the surface should be approximately 1.7 times greater than the measured velocity shown in Figure 9.

The first example of measured boat wake (Figures 9A and B) had peak horizontal and vertical components of the orbital velocity of nearly 0.35 and 0.10 m/s at a 0.6-m water depth (or 0.60 and 0.17 m/s at the surface), respectively. The vessel transited the dredge plume around 13:42 local time, shortly after the turbidity peaked at 13:37 local time. As shown in Figure 7, the turbidity was decreasing rapidly when the vessel crossed the study site. The relative energetic conditions generated by that instance of boat wake had little to no influence on the sediment concentration and its temporal variation. The acoustic signal strength of the ADV data did not respond, in a similar way as the orbital velocities, to the energetic conditions generated by the boat wake. Figure 9B

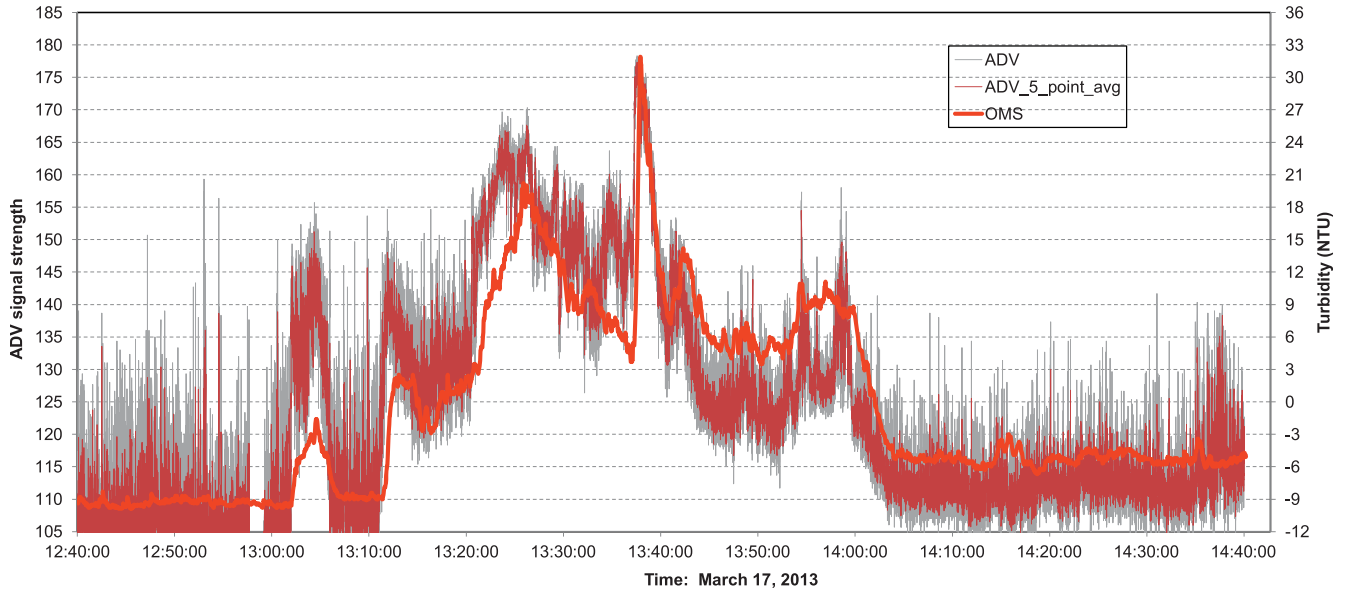

Figure 8. Comparison of the Nortek ADV acoustic signal strength (8-Hz data and 5-point moving averaged) with the 0.5-Hz YSI OMS 600 turbidity measurements. Note the similar overall patterns. (Color for this figure is available in the online version of this paper.)

illustrates the sediment concentrations measured by the colocated OMS Sensor 1 (sampling at 0.5 Hz) over a slightly longer period. A small increase in sediment concentration was measured after the boat passage. However, it is not clear whether this small variation is related to the boat wake, because similar variations occurred throughout the record (Figure 7) and most variations occurred without vessel traffic except for that of the slow-moving dredge, which generated minimal wake. The second example (Figures 9C and D) illustrates a less energetic boat wake following the lower concentration peak around 13:26 local time (Figure 7). The peak boat wake generated horizontal and vertical orbital velocities 0.2 and 0.1 m/s at a 0.6-m water depth (or 0.34 and 0.17 m/s at the surface), respectively. The acoustic signal strength of the ADV measurements did not respond to the boat wake–generated orbital velocities. The trend of change of the sediment concentration, as measured by the OMS sensor over a longer period (Figure 9D), was also not altered by the boat wake. This suggests that the subsidence of the dredge sediment plume was not significantly influenced by the relatively energetic conditions generated by the frequent passages of vessels.

Entrainment of Sediments from the Bottom

The negligible variations in measured sediment concentrations during the passage of vessels indicated a lack of evidence for particle entrainment, or pickup, of either *in situ* sediment or recently deposited dredged sediment. Photos and videos from the underwater camera did not illustrate sediment resuspension from the bottom by boat wake, which corresponded with the lack of increased sediment concentration measured in the water column. Based on the studies by Komar and Miller (1973, 1975), sediment entrainment by wave motion can be estimated as

$$\frac{(U_{\delta\_cr})^2}{(s-1)gd} = 0.21\left(\frac{2A_{\delta\_cr}}{d}\right)^{0.5} \quad \text{for} \quad d_{50} < 0.5\text{mm} \tag{3}$$

where A_δ and U_δ are the maximum near-bottom orbital velocity (in meters per second) and excursion (in meters), respectively; δ is the thickness of the wave boundary layer (in meters); and the subscript *cr* denotes the critical value for the initiation of sediment motion. In addition, s is the sediment specific density (dimensionless) and equals ρ_s/ρ, where ρ is the fluid density and ρ_s is the sediment density (in kilograms per cubic meter), and d is the sediment grain size (in meters). Based on linear wave theory, A_δ and U_δ can be calculated as

$$A_\delta = \frac{H}{2\sinh\left(\frac{2\pi h}{L}\right)} \tag{4}$$

$$U_\delta = \omega A_\delta = \frac{\pi H}{T\sinh\left(\frac{2\pi h}{L}\right)} \tag{5}$$

where H is the wave height (in meters), ω ($2\pi/T$) is the angular velocity (in reciprocal seconds), T is the wave period (in seconds), and h is the water depth (in meters). Substituting Equations (4) and (5) into Equation (3), Soulsby (1997) obtained a formula that directly estimates the critical near-bottom velocity:

$$U_{\delta\_cr} = [0.118g(s-1)]^{\frac{2}{3}} d^{\frac{1}{3}} T^{\frac{1}{3}} \quad \text{for} \quad d_{50} < 0.5\text{mm} \tag{6}$$

Based on Equation (6), sediment entrainment velocity is proportional to sediment grain size and wave period. The average period of the boat-generated waves during the 3-hour study (Figure 10) was 2.08 seconds. Table 1 lists the critical sediment entrainment velocity for various grain-size fractions of bottom sediment (Figure 3) calculated using the average

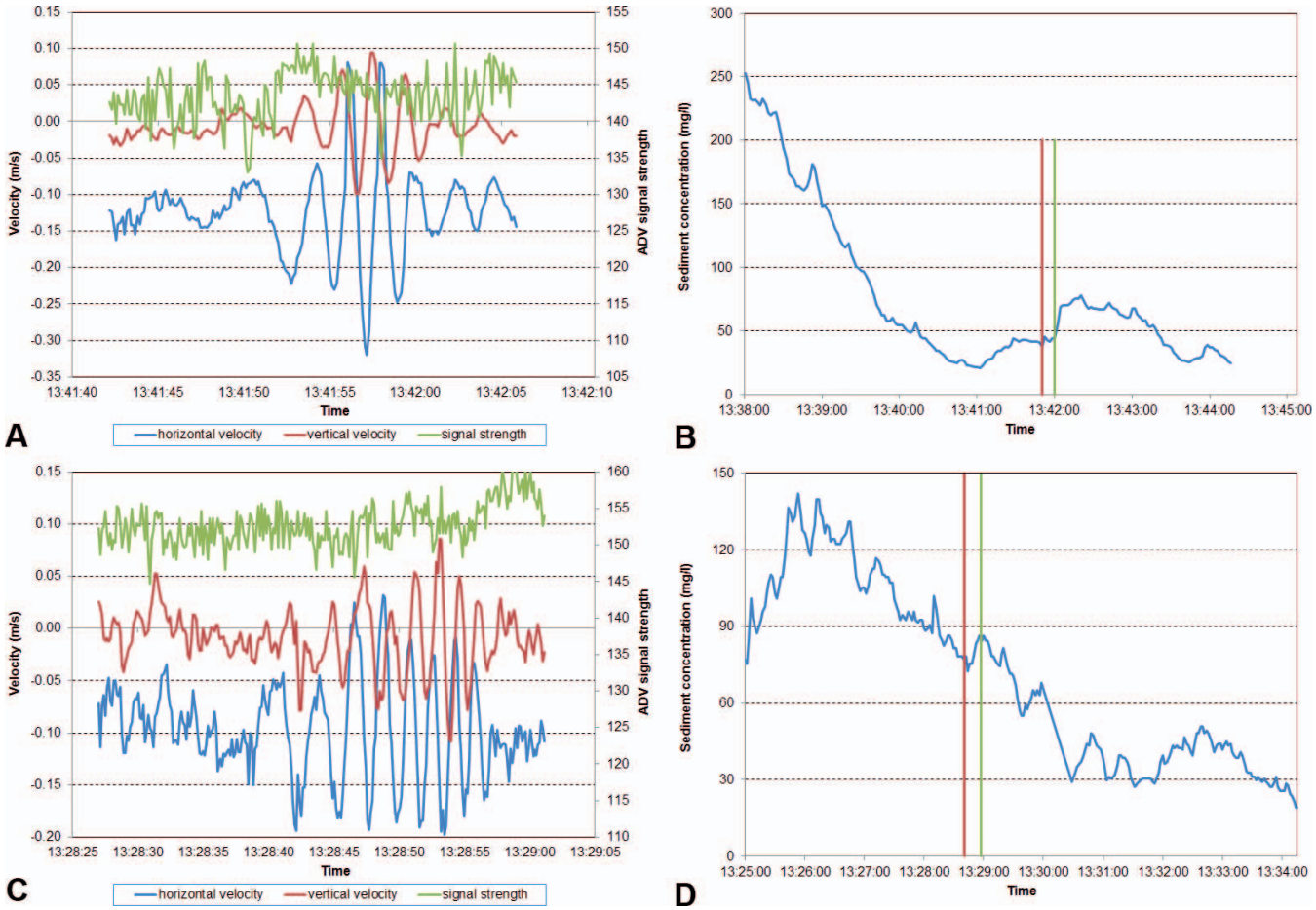

Figure 9. Boat wake–induced energetic conditions and associated turbidity change. (A) An example of boat wake–induced horizontal and vertical oscillatory velocities and corresponding acoustic signal strength, measured at 8 Hz. (B) Turbidity variations during the passage of the boat. The two vertical lines indicate the time of the boat wake passage. (C) Another example of boat wake–induced horizontal and vertical oscillatory velocities and corresponding acoustic signal strength, measured at 8 Hz. (D) Turbidity variations during the passage of the boat. The two vertical lines indicate the time of the boat wake passage. The measurements were conducted around 0.6 m below water surface.

period. It is acknowledged here that Equations (3) and (6) assume a flat sandy bed. Presently, little is known about sediment entrainment over seagrass beds. Although Equation (3) does not represent a comprehensive set of processes, it should provide a conservative estimate of potential sediment entrainment under oscillatory wave motion. It is reasonable to assume that the frictional factor of a seagrass bed should substantially retard the near-bottom fluid motion and anchor bottom sediments, resulting in overestimation by Equation (3).

Sunday afternoon is typically an active recreational boating time throughout the study area. Figure 10 illustrates the vessel-generated waves between 12:00 to 15:00 local time on March 17 2013, extending from shortly before, through during, and to shortly after the dredging operation. The wave heights illustrated in Figure 10 have been corrected for depth attenuation using Equations (1) and (2) and represent wave height at the water surface. During the 3-hour period, 32 significant vessel wake events were measured, or on average a boat passage every 6 minutes. This should represent peak boating activity. The maximum wave heights generated by the vessel passages ranged from 0.06 to nearly 0.30 m, with the wave period ranging from 1.63 to 2.88 seconds. A wake set included several waves generated by each vessel passage (Figure 9), and Figure 10 illustrates the highest wave in each sequence and the associated wave period. The boat-generated waves were higher than the local wind-generated waves.

The maximum near-bottom orbital velocity and excursion, A_δ and U_δ, respectively, associated with boat waves (Figure 10) were calculated based on Equations (4) and (5). Similar to the case of Equation (3), the influence of seagrasses on the near-bottom fluid motion is not considered in Equations (4) and (5). There is no broadly accepted method to incorporate seagrass influence. The calculated A_δ and U_δ values were compared with the critical values estimated from Equation (3) without considering the presence of the seagrasses. The results are illustrated in Figure 11. The entrainment velocities and excursion distances calculated from Equation (3) for three grain-size fractions, d_5, d_{50}, and d_{95}, are also illustrated. For

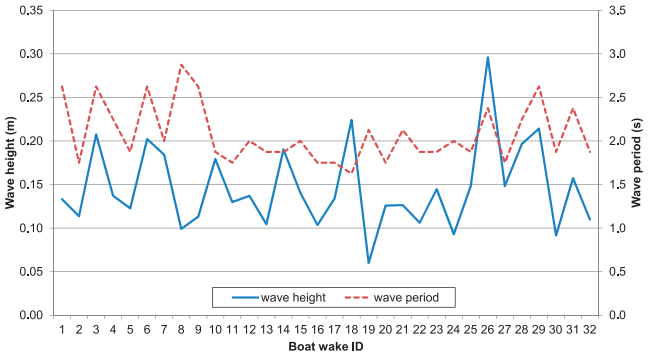

Figure 10. Maximum wave height and associated wave period generated by vessel passages during the 3 hours of data collection. (Color for this figure is available in the online version of this paper.)

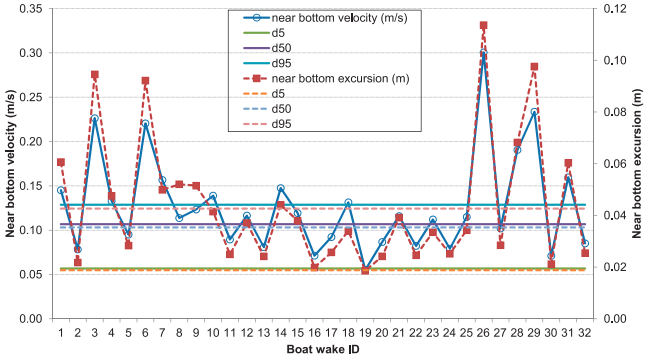

Figure 11. Calculated near-bottom maximum orbital velocity and excursion associated with boat-generated waves. Critical velocities and excursion for the entrainment of three grain-size fractions are also plotted. (Color for this figure is available in the online version of this paper.)

the smaller grain size d_5, the critical velocity and excursion were exceeded by almost all maximum boat wake waves. For median grain size d_{50}, 17 of the 32 boat wake events (53%) created near-bottom current velocity and excursion that exceeded the critical values for entrainment. For the coarser grain size d_{95}, 9 of 32 boat wake events (28%) exceeded the critical values. However, the underwater photos and videos did not show significant sediment resuspension associated with some of the largest boat wakes, and there was negligible to no variation in the suspended-sediment concentration measured by the OMS sensors. This can be attributed to two factors. First, the seagrasses significantly retarded the near-bed fluid motion, resulting in unrealistic estimates from Equations (3) through (5). Second, the slight exceedance of the critical values by the boat wake did not result in significant sediment resuspension that can be identified from the data.

Settling of the Suspended Sediments

Hallermeier (1981) proposed a set of commonly used empirical formulas for calculating settling velocities, assuming that the sediments are noncohesive:

$$w_s = \frac{\nu D_*^3}{18d} \quad \text{for} \quad D_*^3 \le 39 \tag{7}$$

$$w_s = \frac{\nu D_*^{2.1}}{6d} \quad \text{for} \quad 39 < D_*^3 < 10^4 \tag{8}$$

$$w_s = \frac{1.05\nu D_*^{1.5}}{d} \quad \text{for} \quad 10^4 \le D_*^3 < 3 \times 10^6 \tag{9}$$

where w_s is the settling velocity (in meters per second), ν denotes the dynamic viscosity (in kilograms per meter per second), and D_* is the dimensionless grain size, defined as follows:

$$D_* = \left[\frac{(s-1)gd^3}{\nu^2}\right]^{\frac{1}{3}} \tag{10}$$

Soulsby (1997) reanalyzed a large amount of existing data on settling velocities and developed a formula for calculating settling velocity:

$$w_s = \frac{\nu}{d}\left[\left(10.36^2 + 1.049D_*^3\right)^{\frac{1}{2}} - 10.36\right] \tag{11}$$

Equation (11) was verified over a large range of sediment grain sizes, assuming that the sediment is noncohesive (Soulsby, 1997). Cohesive sediments and associated flocculation are not considered by the Hallermeier (1981) and Soulsby (1997) formulas. Given that the study area is mostly composed of sand-size noncohesive sediment with less than 2% mud-size particles (Figure 3), the Hallermeier (1981) and Soulsby (1997) formulas should be applicable.

The settling velocity of sediment in the study area is calculated and plotted in Figure 12A. The time needed for the sediment to settle through a 1.4-m water column, which is used here to represent relatively deeper water, *e.g.*, at the edge of the channel, over the seagrass beds in the study area at high tide is plotted in Figure 12B. About 95% of the sediments that are relevant in the study area should settle through the water column within 1 hour. Actually, 90% of the sediment should settle through the water column within 5 minutes based on the computed settling velocity. This agrees in general with observations from this study. Both the Hallermeier (1981) and Soulsby (1997) formulas, as is the case for most settling velocity equations, calculate sediment settling through tranquil water. Settling in natural environments may be hindered

Table 1. *Critical sediment entrainment velocity for various grain-size fractions of bottom sediment calculated using the average boat wake period of 2.08 seconds.* d_5 *represents the fifth percentile grain size from the fine end of the grain-size distribution. The percentile increases toward the coarse end.*

Grain-Size Fraction	d_5	d_{10}	d_{15}	d_{25}	d_{50}	d_{75}	d_{85}	d_{90}	d_{95}
Grain Size (mm)	0.024	0.092	0.105	0.123	0.159	0.201	0.225	0.247	0.279
A_{δ_cr} (m)	0.019	0.029	0.031	0.032	0.035	0.038	0.040	0.041	0.043
U_{δ_cr} (m/s)	0.057	0.089	0.093	0.098	0.107	0.115	0.120	0.124	0.129

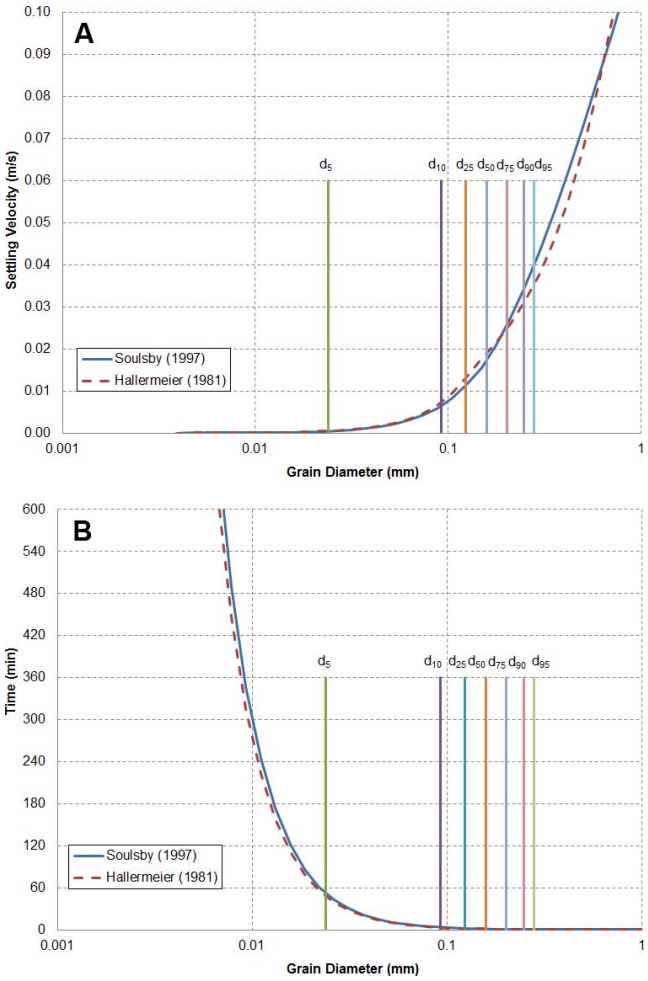

Figure 12. (A) Settling velocity *vs*. sediment grain size calculated based on Soulsby (1997) and Hallermeier (1981) formulas. (B) Time needed to settle through a 1.4-m water column for various sediment grain sizes. (Color for this figure is available in the online version of this paper.)

by dynamic conditions, such as turbulent motion associated with waves and currents. For the case here, wave- and current-induced turbulence does not seem to have significantly changed the settling of the sediment because the observed time of turbidity subsidence is on the same order of magnitude as the calculated time (Figure 12). For example, the two measured turbidity peaks (Figure 7) both lasted approximately 3 to 8 minutes. This suggests that hindering the settling induced by the hydrodynamic conditions did not fundamentally change the overall trend of settling. In addition, the dense seagrasses within the study area should substantially prevent the resuspension of the sediment once settled on the bottom. Given that seagrass beds tend to occur in areas with relatively calm conditions (Robert, Matthew, and Graeme, 2006), sediment resuspension, as well as dynamic hindering of settling, should not be a significant factor in general. Based on the calculated settling velocity and the field observations, dredge plumes should settle within 1 hour over shallow and moderately, well-sorted fine sand substrates, which are common in the relatively quiescent back-barrier water bodies along the Gulf Coast of peninsular Florida.

The settling time of the dredge plume (or plume collapse time) measured and calculated by this study is on the same order of magnitude, *i.e*. around 1 hour, as the time summarized in Pennekamp *et al*. (1996). In terms of impacts on seagrass beds, Erftemeijer and Lewis (2006) cautioned that criteria developed in one geographic area might not be directly applicable to other areas. Site-specific data and understanding are crucial in evaluating possible impacts. Furthermore, even though the suspended sediments induced by dredging settled quite quickly, it cannot be directly implied that no stress to the seagrasses may have occurred. Some settled sediments could accumulate on the blades of the seagrasses and could reduce photosynthesis, depending on how long they remain on the surface of the blades.

CONCLUSIONS

Turbidity increase associated with an IWW dredging operation in west-central Florida and subsequent dredge plume subsidence were measured in the field, along with measurements of *in situ* wave and current conditions. Sediment in the study area is dominantly composed of fine sand with less than 2% mud-size particles. The dredge plume temporarily increased the turbidity to more than 400 mg/L and substantially reduced the visibility to less than 0.5 m. The settling of the dredge plume can be calculated rather accurately with commonly used settling velocity formulas for noncohesive sediments (*e.g*., Hallermeier, 1981; Soulsby, 1997). Because the seagrass beds typically distribute in water depths of less than 2 m, the fine, sand-size particles were found to settle to the bed mostly within 1 hour. The calculated settling time generally agreed with the field data. Therefore, reduction of light penetration caused by dredging-induced turbidity increases is limited to about a 1 hour for the study area. The relatively energetic conditions generated by the frequent boat wakes, despite slightly exceeding the calculated sediment entrainment threshold, did not result in significant resuspension and remixing of the suspended sediments and had minor influence on the settling time of the dredge plume.

ACKNOWLEDGMENTS

This study is funded by the U.S. Army Engineer Research and Development Center and the University of South Florida. Field data collection was assisted by Deborah Shafer, Cheryl Pollock, Coraggio Maglio, Mark Horwitz, and Ming Xie. Permission to publish this paper was granted by USACE headquarters.

LITERATURE CITED

Erftemeijer, P.L.A. and Lewis, R.R., 2006. Environmental impacts of dredging on seagrasses: A review. *Marine Pollution Bulletin,* 52(12), 1553–1572.

Hallermeier, R.J., 1981. Terminal settling velocity of commonly occurring sand grains. *Sedimentology,* 28(6), 859–865.

Koch, E.W., 2001. Beyond light: Physical, geological, and geochemical parameters as possible submersed aquatic vegetation habitat requirements. *Estuaries,* 24(1), 1–17.

Komar, P.D. and Miller, M.C., 1973. The threshold of sediment movement under oscillatory water waves. *Journal of Sedimentary Petrology,* 43(4), 1101–1110.

Komar, P.D. and Miller, M.C., 1975. On the comparison between the threshold of sediment motion under waves and unidirectional currents with a discussion of the practical evaluation of the threshold. *Journal of Sedimentary Petrology,* 45(2), 362–367.

Moore, K.A.; Wetzel, R.L., and Orth, R.J., 1997. Seasonal pulses of turbidity and their relations to eelgrass (*Zostera marina L.*) survival in an estuary. *Journal of Experimental Marine Biology and Ecology,* 215(1), 115–134.

Onuf, C.P., 1994. Seagrasses, dredging and light in Laguna Madre, Texas, U.S.A. *Estuarine, Coastal and Shelf Science,* 39(1), 75–91.

Pennekamp, J.G.S.; Epskamp, R.J.C.; Rosenbrand, W.F.; Millie, A.; Wessel, G.L.; Arts, T., and Deibel, I.K., 1996. Turbidity caused by dredging; viewed in perspective. *Terra et Aqua,* 64, 10–17.

Perkey, D.; Pratt, T.C., and Ganesh, N.B., 2010. Comparison of SSC measurements with acoustic backscatter data: West bay sediment diversion, Mississippi River. *Proceedings of the 2nd Joint Federal Interagency Conference* (Las Vegas, Nevada).

Ralph, P.J.; Tomasko, D.; Moore, K.; Seddon, S., and Macinnis-Ng, C.M.O., 2006. Human impacts on seagrasses: Eutrophication, sedimentation, and contamination. *In:* Larkum, A.W.D.; Orth, R.J., and Duarte, C. (eds.), *Seagrasses: Biology, Ecology and Conservation*. Dordrecht, The Netherlands: Springer, pp. 567–593.

Robert, J.O.; Matthew, C.H., and Graeme, J.I., 2006. Ecology of seagrass seeds and seagrass dispersal processes. *In:* Larkum, A.W.D.; Orth, R.J., and Duarte, C. (eds.), *Seagrasses: Biology, Ecology and Conservation*. Dordrecht, The Netherlands: Springer, pp. 111–133.

Schoellhamer, D.H., 2002a. Anthropogenic sediment resuspension mechanisms in a shallow microtidal estuary. *Estuarine, Coastal and Shelf Science,* 43(5), 533–548.

Schoellhamer, D.H., 2002b. Comparison of the basin-scale effect of dredging operations and natural estuarine processes on suspended sediment concentration. *Estuaries,* 25(3), 488–495.

Shafer, D.J., 1999. The effects of dock shading on the seagrass *Halodule wrightii* in Perdido Bay, Alabama. *Estuaries,* 22(4), 936–943.

Soulsby, R., 1997. *Dynamics of Marine Sands*. London: Thomas Telford, 272p.

USACE (U.S. Army Corps of Engineers) Staff, 2015. *Dredging and Dredged Material Management*. Vicksburg, Mississippi: U.S. Army Corps of Engineers Publication, *Engineering Manual EM 1110-2-5025*. http://www.publications.usace.army.mil/Portals/76/Publications/EngineerManuals/EM_1110-2-5025.pdf.

Wang, P. and Beck, T.M., 2012. Morphodynamics of an anthropogenically altered dual-inlet system: John's Pass and Blind Pass, west-central Florida, USA. *Marine Geology,* 291–294, 162–175. doi:10.1016/j.margeo.2011.06.001

Wang, P. and Stone, G.W., 2004. Nearshore wave measurement. *In:* Schwartz, M. (ed.), *Encyclopedia of Coastal Science*. Dordrecht, The Netherlands: Springer, pp. 869–874.